Catalysis Today 175 (2011) 552–557

Contents lists available at ScienceDirect

Catalysis Today

journal homepage: www.elsevier.com/locate/cattod

Characterization of oxidation and reduction of a platinum–rhodium alloy by atom-probe tomography

Tong Li[a,*], E.A. Marquis[a,b], P.A.J. Bagot[a], S.C. Tsang[c], G.D.W. Smith[a]

[a] Department of Materials, University of Oxford, Parks Road, Oxford OX1 3PH, United Kingdom
[b] Department of Materials Science and Engineering, University of Michigan, Ann Arbor, MI 48109, USA
[c] Wolfson Catalysis Centre, Department of Chemistry, University of Oxford, Oxford OX1 3QR, United Kingdom

ARTICLE INFO

Article history:
Received 19 October 2010
Received in revised form 28 February 2011
Accepted 16 March 2011
Available online 22 April 2011

Keywords:
Pt–Rh
Oxidation
Reduction
Atom-probe tomography
Diffusion

ABSTRACT

An active challenge in heterogeneous catalysis is to minimize the quantities of the expensive platinum group metals used without causing degradation of the overall catalytic efficiency in a chemical reaction. To achieve this goal, a thorough atomic-scale understanding of these materials under reactive conditions is required. This will enable the design and production of "nano-engineered" catalysts, optimised for cost, stability and performance. In this study, the oxidation and reduction behaviour of a Pt–Rh alloy between 873 and 1073 K was investigated by atom-probe tomography (APT). Detailed observations of the concentration profiles at the oxide/metal interfaces show that the growth of Rh_2O_3 oxide is limited by diffusion of Rh in the alloy. By varying the oxidation conditions, it was possible to calculate the activation energy for Rh diffusion in Pt–Rh as 236 ± 41 kJ/mol, together with diffusion coefficients for Rh for a range of temperatures. Reduction of the oxide phase left a thin, almost pure, layer of the most reactive (and expensive) element, Rh, on the surface of the specimen, suggesting a simple route for engineering the formation of the core–shell structure Pt–Rh nanoparticles.

1. Introduction

Platinum and rhodium are two important metals in heterogeneous catalysis, extensively utilized together, for example in automobile exhaust emission control and ammonia oxidation. These elements, along with other platinum group metals (PGMs) are highly successful catalysts in a wide range of applications owing to their superior activity and stability in harsh operating environments. These environments can often be strongly oxidizing, and the catalytic performance can be heavily influenced by the oxidation state of the PGM surface. Additionally, the atomic-scale structure and surface composition of the catalyst may be altered during the various stages of a reaction. Investigating how the environment can drive changes on catalyst surfaces is therefore critically important, both for a fuller understanding of these important materials and to enable catalyst manufacturers to produce future performance improvements. In this study, we have investigated the changes to a Pt–Rh alloy following exposure to oxidizing/reducing environments using atom-probe tomography (APT), a unique method for probing the chemical structure of materials at the atomic scale.

PGMs can demonstrate markedly different catalytic properties when oxidized [1–3]. At a fundamental level, the surface composition of alloy catalysts can often differ from the bulk, and these changes can be driven in often opposing directions by thermal effects or adsorbates. Previous studies of PGM oxidation have mainly focused on the investigating the stoichiometry, structure and volatility of oxides phases formed using conventional characterization techniques. These techniques include gravimetric analysis [4,5], X-ray diffraction [6], low energy electron diffraction (LEED) [7], X-ray photoelectron spectroscopy (XPS) [8,9] and scanning electron microscopy (SEM) [10]. However, in order to better control the behaviour of platinum group metal nanoparticles under catalytic conditions, a more detailed understanding of oxidation processes at the atomic scale is required, which will provide a basis for how the catalyst surfaces can be modified. Oxygen-induced Rh surface segregation in Pt–Rh alloys has been seen using a range of surface science techniques including auger electron spectroscopy (AES), XPS, and low energy ion scattering (LEIS) [9,11–16]. Field ion microscopy (FIM) experiments have revealed catalytic oscillations in the reaction of gases on nanosized PGM surfaces [17–19], while scanning tunnelling microscopy (STM) studies have also shown that these type of oscillations in reactive environments can reconstruct the metal surfaces [20]. Moreover, industrial catalysts have also demonstrated significant reconstruction during operation [21,22].

* Corresponding author. Tel.: +44 1865 273 711; fax: +44 1865 273 789.
E-mail address: tong.li@materials.ox.ac.uk (T. Li).

0920-5861/$ – see front matter © 2011 Elsevier B.V. All rights reserved.
doi:10.1016/j.cattod.2011.03.046

Early atom-probe studies revealed the deep level of understanding of the crystallographic and spatial aspects of surface oxidation and segregation that is obtainable by using atomic-scale methods [23–25]. More recent APT studies by the Oxford group reported surface composition changes to Pt–Rh, Pt–Rh–Ru and Pt–Rh–Ir alloys after oxidation, with the extent dependent on the crystallographic surface investigated [26–29]. In many of these experiments, the oxidation conditions were constrained to lower temperatures/pressures due to practical limitations. Thus a quantitative, atomic-scale investigation of surface composition changes to platinum alloys at high temperatures, up to those relevant to ammonia oxidation [30], is desired in order to understand how catalyst particles may be modified during service in commercial systems.

APT is ideally suited for the atomic-scale analysis of metal/oxide systems in a wide range of materials [31]. The geometry of the specimen is advantageous, as the needle-shaped apex has a radius of curvature of <100 nm. The apex region is therefore a good model for a catalyst nanoparticle; approximately double its size and with a similar curved structure. In this paper, we report on the severe oxidation of a Pt–Rh alloy at temperatures between 873 and 1073 K. We also determine an activation energy and diffusion coefficients for Rh diffusion in the Pt–Rh alloy. Finally, we study the structure of oxidized samples following reduction in hydrogen, demonstrating that such treatments could be used as a method of nano-engineering catalyst surfaces with different compositions from the bulk alloy.

2. Materials and methods

A Pt–22 at.% Rh alloy in the form of as-drawn wire (0.1 mm diameter) was obtained from Alfa-Aesar. APT specimens were prepared by electropolishing using a molten salt mixture of 4:1 $NaNO_3$:NaCl heated in an electrical salt pot to 700–750 K. The specimens were subsequently cleaned of any residual surface oxide by field evaporation of the first few atomic layers before being exposed to any oxidizing treatment. For all specimens, the [1 0 0] direction was parallel to the specimen axis. Following preparation and cleaning, specimens were oxidized at 873 K, 973 K or 1073 K for 5 h in 1 bar of oxygen at a flow rate of 35 cm^3/min. In a separate set of experiments, several specimens were oxidized at 1073 K for 1 h in oxygen, and then reduced at 673 K for 1.5 h in 1 bar of hydrogen.

Transmission electron microscopy (TEM), carried out using a Philips CM20 microscope operated at 200 kV, was used to observe selected specimens pre- and post-oxidation. Specimens were characterized by APT using a Cameca LEAP 3000X-HR^{TM} instrument. Several specimens were analysed for each unique thermal/gas exposure. The analyses were carried out in laser pulsing mode with a specimen temperature of 55 K, target evaporation rate of 2 ions per 1000 pulses, pulse rate of 160 kHz, pulse energy of 0.5 nJ and a laser spot size of approximately 10 μm. The standing voltage was automatically increased in order to maintain a constant evaporation rate. Compositional analyses of the as-received materials by APT yielded a Rh content of 22.6 ± 0.42 at.% compared with the nominal composition of 22.07 at.%. The different reconstruction parameters (image compression factor, evaporation field, radius and field factor) can have a significant influence on the scale and aspect ratio of the 3D reconstructions and therefore any quantitative measurement of distances. In this study, the values of the image compression factor and the field factor were kept as the default values (1.65 and 3.3) of the reconstruction procedure. The evaporation field was set at 30 V/nm, by considering the observed ratios of Pt^{1+}:Pt^{2+}. The scaling errors affecting length scale measurements and introduced by inaccurate reconstruction parameters were estimated assuming a possible 20% variation in the estimation of the specimen end radius.

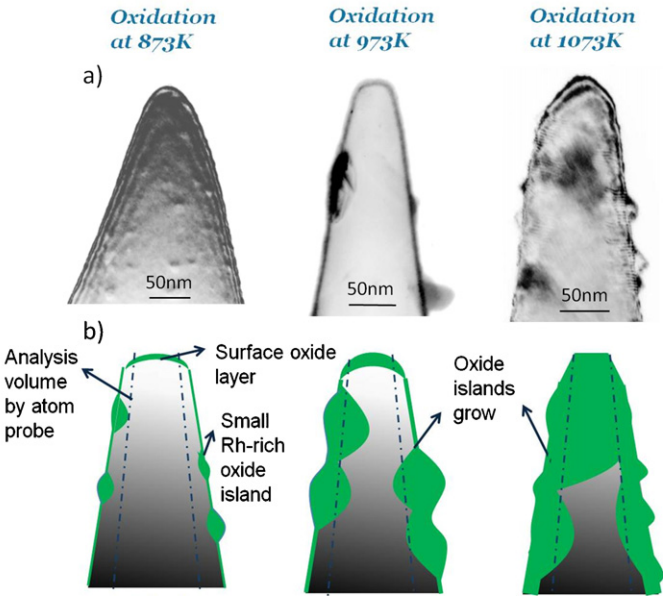

Fig. 1. (a) TEM images of oxidized atom probe specimens and (b) schematic representations of oxidation process on APT specimens at 873–1073 K. Dashed lines indicate approximate analysis volume in APT.

3. Results

3.1. Morphology observations

The formation of oxide phases was identified by both APT and TEM at the three chosen oxidizing temperatures. After oxidation at 873 K for 5 h, the oxide phase nucleated on the surface of the specimens in the form of small islands, as revealed by the TEM image in Fig. 1a. A thin oxide layer also formed on the surface of the specimens, which is captured by the APT analysis (Fig. 2a). In these atom maps, each dot represents an individual ion or ionic species, with those at the top of the map coming from the apex of the specimen. The maps are divided into three separate volumes to highlight the different oxygen species, oxides and metallic ions detected. Note that due to the limited field of view of the atom probe instrument, only the central part of the specimen is examined. To aid explanation of the APT data, Fig. 1b shows a schematic representation of the oxidation process at the three different temperatures. The blue dashed lines in the schematics of Fig. 1b represent the volumes analysed by APT. The oxide regions evaporate in the form of O ions and molecular ion complexes (RhO_x and PtO_y). After oxidation at 973 K, oxide crystals formed with slightly larger sizes (~30 nm), and appear to protrude from the surface with elongated shapes (Fig. 1b). Some of the oxide islands have also grown inward sufficiently to be captured within the APT field of view. The analysis shown in Fig. 2b suggests the presence of two main islands of oxide, on the apex and the shank. At the highest oxidation temperature of 1073 K, specimens showed an even greater level of oxidation, as revealed by the TEM image in Fig. 1c. A thicker oxide region is also noticeably evident in the atom probe data of Fig. 2c.

In these experiments, we are mainly interested in the development of the oxide/metal interfaces within the near surface or bulk regions of the specimens. However, it is certainly possible that under the oxidation conditions employed diffusion of oxide species *across* the specimen surface is also occurring, for example from the shank to the apex. This behaviour has been previously identified

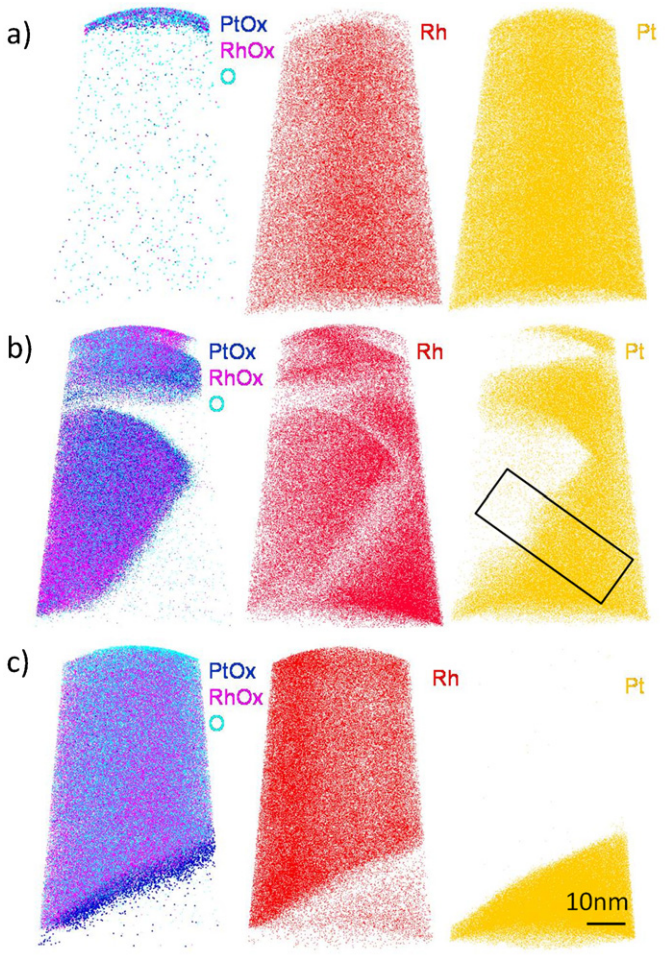

Fig. 2. APT reconstructions of oxidized atom probe specimens showing the spatial distributions of RhO_x, PtO_y, Rh and Pt ionic species for the three oxidation temperatures: (a) 873 K (b), 973 K and (c) 1073 K.

[32], while the complex diffusion of atoms over the apex itself has also been explored using APT [26,27]. In the current study however we believe these processes will have little influence on the nature of the oxide/metal interfaces formed here. Finally, note that PtO_x species were sometimes detected preferentially at the oxide/metal interface. These are thought to be artefacts of evaporation as previously reported in oxide/metal systems [33] but they do not change the measured compositions.

3.2. Composition of oxide phases

Detailed analyses of the oxide phase and the oxide/metal interface were performed using proximity histograms [34]. A representative histogram for a specimen oxidized at 873 K for 5 h is shown in Fig. 3, calculated based on an iso-concentration surface of 35 at.% O. An iso-concentration surface is a planar construct, located at the metal–oxide interface. The proximity histogram is perpendicular to this plane, and classifies species through the iso-concentration surface by chemical identity. For clarity, we choose to group species as Rh, Pt, and O, independent of the PGM oxidation states. Three distinct regions are visible: the oxide phase on the right-hand side, the bulk alloy region (Pt–22 at.% Rh) on the left-hand side and a 2–3 nm thick intermediate Rh-depleted region approaching the oxide/metal interface. The composition of the oxide phase changes slightly with temperature. Decreasing levels of Pt are apparent with increasing oxidation temperature. Table 1 summarizes the oxide compositions. For all temperatures,

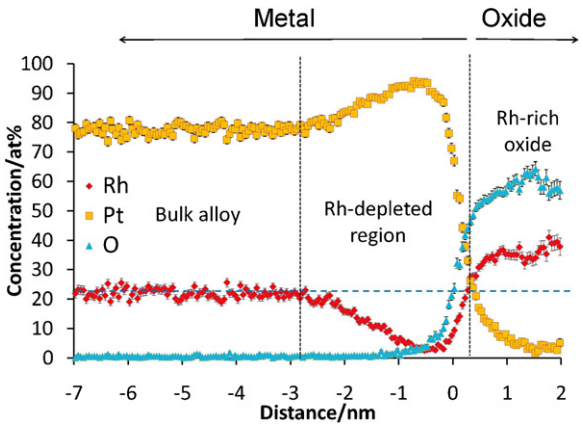

Fig. 3. Proximity histogram obtained from a specimen oxidized at 873 K for 5 h. The iso-concentration surface is located approximately 2.9 nm from the Pt–Rh surface.

Table 1
Rh and Pt concentrations in the oxide layer.

Temperature (K)	873	973	1073
Rh (at.%)	35.57 ± 0.70	38.39 ± 0.46	40.54 ± 0.16
Pt (at.%)	6.61 ± 0.30	2.02 ± 0.11	0.04 ± 0.01

the measured stoichiometry is consistent with that of M_2O_3 where M = Rh + Pt.

With increasing oxidation temperature, the depth of the Rh depleted region at the oxide/metal interface increases sharply. Fig. 4 shows the profiles for the Rh concentration near the oxide/metal interface for all three oxidation temperatures. At 1073 K, the width of the depleted region is larger than the length of the atom probe analysis.

3.3. Time-dependence of oxide formation

A number of Pt–Rh specimens were oxidized at 973 K for 1.25 h, 2.5 h or 5 h to follow the kinetics of oxide growth. Based on proximity histograms, the Rh concentration in the oxide layer showed little deviation over 1.25 h, 2.5 h and 5 h, remaining around 37–39 at.%. However, the depths of the Rh-depleted layers clearly differed, and these were quantified by measuring the distances from the point with the lowest Rh concentration to where the nominal Rh concentration was recovered (Fig. 5). The Rh depleted layers after the oxidation treatment for 1.25 h, 2.5 h and 5 h were therefore 6.70 nm, 9.65 nm and 14.50 nm in depth, respectively.

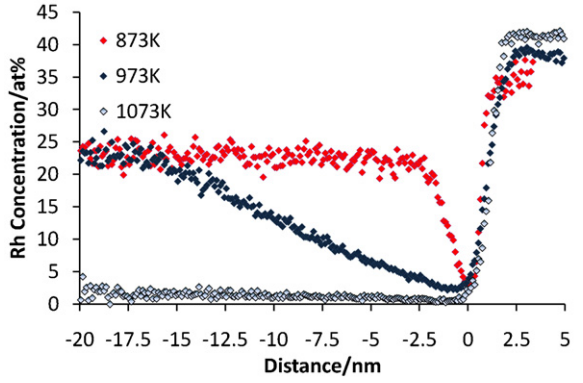

Fig. 4. Rh concentration profiles at the oxide/metal interfaces (from proximity histograms) after oxidation at 873, 973 and 1073 K for 5 h. The black box in Fig. 2b illustrates the corresponding (fixed) sampling volume for 973 K.

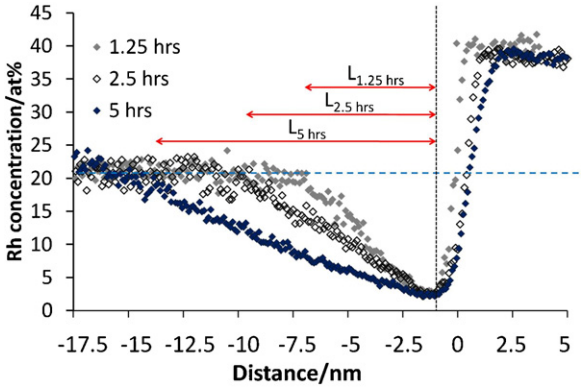

Fig. 5. Rh concentration profiles at the oxide/metal interfaces (from proximity histograms) after oxidation at 973 K for 1.25, 2.5 and 5 h.

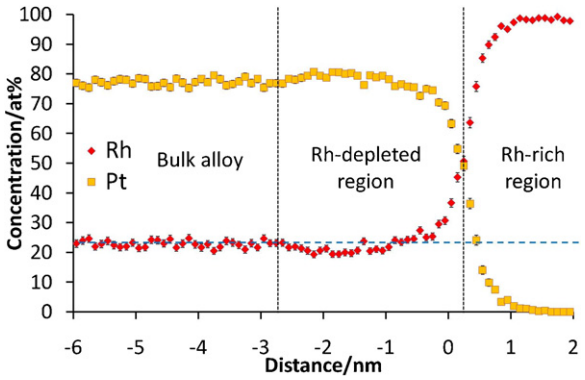

Fig. 7. Proximity histogram obtained from specimen shown in Fig. 6. The iso-concentration surface is located approximately 3.2 nm from the Pt–Rh surface.

3.4. Oxidation/reduction on Pt–Rh

Following the oxidation treatment at 1073 K for 1 h, three separate specimens were subsequently reduced in H_2. After reduction at 673 K for 1.5 h, a 2 nm thick, an almost pure Rh-rich outer metallic layer was observed, as illustrated in Fig. 6. This result was consistent over all oxidation/reduction experiments under these conditions. Note also that the depth of the Rh enriched region is in qualitative agreement with that identified for the oxidation at 973 K for 1.25 h (proxigram shown in Fig. 5). In this a Rh enriched oxide layer of approximately 3–4 nm was apparent. A small amount of atomic oxygen remains on the surface of the reduced specimen, which may be due to chemisorption during transfer of the specimen from the oxidation furnace to the atom probe analysis chamber. The composition of the reduced layer is 99.6 ± 1.3 at.% Rh–0.4 ± 0.1 at.% Pt. Despite the retention of the Rh-enriched layer at the surface, note that the Rh-depleted region at the oxide/metal interface is no longer observed (Fig. 7).

4. Discussion

4.1. Oxidation behaviour

According to the heats of oxide formation reported in the literature (167 kJ/mol for PtO_2 [35], 142 kJ/mol for PtO [36] and 365–405 kJ/mol O_2 for Rh_2O_3 [37]), oxidation of the Pt–Rh alloy should lead to the presence of Rh_2O_3 with perhaps some PtO in the Rh-depleted region immediately beneath this, although Pt oxide has been seen to decompose above ~750 K [38]. Previous studies considering Pt–Rh oxidation have identified oxides heavily enriched in Rh [9,11–16,24], in agreement with the results shown here. The morphologies of the oxide phases observed by TEM also agree with previous published results. Carol and Mann reported that a thin layer of Rh oxide was formed at 873 K with a hexagonal crystal structure [39]. At 973 K, a duplex oxide morphology comprising of a thin layer of hexagonal crystal structure and a thicker layer of orthorhombic crystal structure was found using X-ray diffraction, which is consistent with the greater extent of oxidation apparent at 973 K vs. 873 K demonstrated in Figs. 1 and 2.

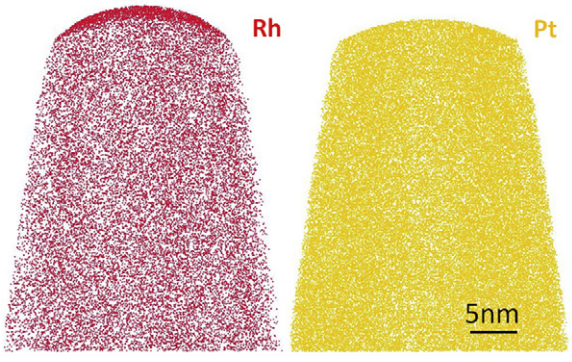

Fig. 6. APT reconstruction after oxidation at 1073 K for 1 h and reduction at 673 K for 1.5 h.

4.2. Diffusion of Rh in Pt

Two main controlling mechanisms are usually considered for oxide growth: diffusion of oxygen through the oxide layer reacting with the metallic species at the oxide/interface, or metal diffusion through the oxide layer so the oxide layer grows at the top oxide surface. In the present case, the development of a Rh depleted layer at the Rh_2O_3/metal interface indicates that the diffusion of Rh on the metal side to the oxide/metal interface is the controlling mechanism for oxide growth. Oxygen diffusion through the oxide layer must therefore occur faster than Rh diffusion in the alloy. The width of the Rh depleted zone provides a measure of the Rh diffusion coefficient in Pt. A basic model for the diffusion of planar interfaces is used [40] and is illustrated in Fig. 8. It is based on the approximation of a static interface, and assumes a mass balance, so the two shaded regions in Fig. 8 are equal:

$$(C_B - C_0)X = \frac{L(C_0 - C_e)}{2} \quad (1)$$

where C_B and C_o are the Rh concentrations in the oxide phase and metal phase respectively, C_e is the (minimum) Rh concentration at the oxide/matrix interface on the metal side, X is the oxide thickness, and L is the diffusion length, i.e. the overall depth of the depleted region within the metal. The flux of Rh atoms across the interface determines the velocity of the interface and is controlled

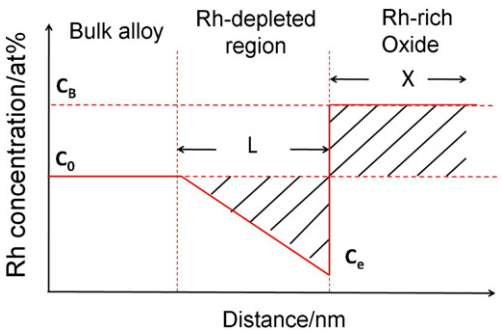

Fig. 8. Schematic diagram illustrating simplified diffusion model.

Table 2
Diffusion coefficients at different temperatures.

Temperature (K)	873	973	1073
$D_{\text{Rh in Pt}}$ (m^2/s)	$1.6 \pm 1.1 \times 10^{-22}$	$5.2 \pm 2.2 \times 10^{-21}$	$7.3 \pm 2.5 \times 10^{-20}$
$D_{\text{Pt in Pt}}$ (m^2/s) from [38]	2.0×10^{-21}	7.4×10^{-20}	1.4×10^{-18}

by diffusion in the metal side (1st Fick's law). From Figs. 4 and 5, the interface is sharp, therefore as derived in [40], the diffusion coefficient of Rh in Pt can be expressed as:

$$D = \frac{(C_B - C_e)L^2}{4(C_B - C_0)t} \quad (2)$$

where L is the diffusion length, determined from the APT data at temperatures from 873 to 1073 K data and t is the oxidation time. The values of concentrations are obtained from the proximity histograms allowing the diffusion coefficients for Rh in Pt at all three oxidation temperatures to be estimated. These values are shown in Table 2. At 973 K, an average value can be estimated from the three oxidation times, with the Rh depletion widths measured from the proximity histograms shown in Fig. 5. From Eq. (2), note that for a fixed diffusion coefficient, the diffusion length L is proportional to the square root of the oxidation time t. This relationship accurately describes the relative changes in diffusion lengths as shown in Fig. 5. The activation energy for Rh diffusion in Pt is obtained by performing this analysis at several temperatures and taking the slope of $\log D$ vs. $1/T$. This yields an activation energy for diffusion of Rh in a Pt–Rh alloy of 236 ± 41 kJ/mol. This value is in close agreement with activation energies for Rh diffusion into different Pt crystal planes as determined from surface studies [41,42].

4.3. Core/shell structure

Creating core/shell structures by surface segregation of one of the components is limited by thermodynamic considerations. In a binary alloy system heated in vacuum, surface segregation of one of the components depends on its surface energy, heat of sublimation, and atomic size [43–45]. Based on these rules, Pt should segregate to the surface in a Pt–Rh alloy in vacuum since the surface energy of Pt (2.48 J/m^2) is lower than for Rh (2.70 J/m^2), while their atomic radii and heats of sublimation are roughly similar [46]. This has indeed been seen experimentally in a number of earlier atom probe studies [23,25]. However, chemisorption of impurities of gaseous species can dramatically change the surface composition. This has also been identified in previous atom probe work, showing that trace amounts of sulphur can lead to Rh enrichment at surfaces in Pt–Rh, Pt–Ir and Pt–Ru alloys [23,25]. In practice, controlling the catalysis environment to drive one or the other element to the surface is not trivial. The rational design of alloy metal nanocatalysts from fundamental principles has the potential to yield catalysts of greatly improved activity and selectivity. A promising area of research concerns the creation of near-surface metal or alloy compositions different from the bulk, which can endow surfaces with novel catalytic properties [47]. The present work illustrates quantitatively a much more straightforward and robust way to create core/shell structures using an oxidation/reduction cycle. The XPS study of Wang and Schmidt demonstrated a Rh-rich surface on Pt–50 at.% Rh alloy particles after an oxidation/reduction cycle [13], while a similar study on the reaction-driven production of core–shell structure nanoparticles was carried out on Rh–Pd and Pt–Pd alloys [48]. The reduction temperature needs be chosen carefully as too low temperatures may yield incomplete reduction, but too high temperatures or excessive exposure times may lead to diffusion of Rh back into the bulk alloy, removing the Rh rich surface layer [13]. Note that the diffusion distance estimated by extrapolating the Rh diffusion coefficient from 873–1073 K to 673 K cannot explain the absence of the Rh depleted region at the oxide/metal interface.

5. Conclusions

The oxidation between 873 and 1073 K and oxidation/reduction behaviour of a Pt–22 at.% Rh alloy in the form of sharp needle specimens was studied using electron microscopy and atom probe tomography. It was found that oxide islands of Rh_2O_3 grow from the apex and the shank of the specimens, and the growth rate is controlled by diffusion of Rh from the bulk to the oxide/metal interface. The Rh depleted region formed allowed the measurement of the activation energy and diffusion coefficients of Rh in Pt. Subsequent reduction of the oxidized specimens at 673 K created core/shell structures consisting of a thin almost pure Rh layer at the surface, above a "core" with the bulk alloy composition. The fundamental study of the surface Rh concentration and quantitative study of Rh diffusivity in Pt will be beneficial to the design of Pt–Rh nanoparticles or pre-treatment of the particles to make the best use of the precious platinum group metals used in heterogeneous catalysts.

Acknowledgements

This work was supported by the UK Engineering and Physical Sciences Research Council (EPSRC) under grant no. EP/077664/1. EAM acknowledges financial support from the Royal Society in the form of a Dorothy Hodgkin Research fellowship.

References

[1] A.S. Aricò, A.K. Shukla, H. Kim, S. Park, M. Min, V. Antonucci, Appl. Surf. Sci. 172 (2001) 33.
[2] R. Pan, W. Yucheng, Q. Wang, W. Hong, Chem. Eng. J. 153 (2009) 206.
[3] R. Westerstrom, J.G. Wang, M.D. Ackermann, J. Gustafson, A. Resta, A. Mikkelsen, J.N. Andersen, E. Lundgren, O. Balmes, X. Torrelles, J.W.M. Frenken, B. Hammer, J. Phys. Condens. Matter 20 (2008) 184018.
[4] J.C. Chaston, Platinum Met. Rev. 8 (1964) 50.
[5] J.C. Chaston, Platinum Met. Rev. 9 (1965) 51.
[6] O. Muller, R. Roy, J. Less-Common Met. 16 (1968) 129.
[7] M. Salmeron, L. Brewer, G.A. Somorjai, Surf. Sci. 112 (1981) 207.
[8] M. Peuckert, Surf. Sci. 141 (1984) 500.
[9] M. Rubel, M. Pszonicka, M.F. Ebel, A. Jabłoński, W. Palczewska, J. Less-Common Met. 125 (1986) 7.
[10] J.C. Chaston, Platinum Met. Rev. 19 (1975) 135.
[11] D.B. Beck, C.L. DiMaggio, G.B. Fisher, Surf. Sci. 297 (1993) 293.
[12] D.B. Beck, C.L. DiMaggio, G.B. Fisher, Surf. Sci. 297 (1993) 303.
[13] T. Wang, L.D. Schmidt, J. Catal. 71 (1981) 411.
[14] R.M. Wolf, J. Siera, F.C.M.J.M. van Delft, B.E. Nieuwenhuys, Faraday Discuss. Chem. Soc. 87 (1989) 275.
[15] B. Moest, S. Helfensteyn, P. Deurinck, M. Nelis, A.W. Denier van der Gon, H.H. Brongersma, C. Creemers, B.E. Nieuwenhuys, Surf. Sci. 536 (2003) 177.
[16] W.B. Williamson, H.S. Gandhi, P. Wynblatt, T.J. Truex, R.C. Ku, AIChE Symp. Ser. 76 (1980) 212.
[17] V.V. Gorodetskii, V.I. Elokhin, J.W. Bakker, B.E. Nieuwenhuys, Catal. Today 105 (2005) 183.
[18] V.V. Gorodetskii, A.A. Sametova, A.V. Matveev, V.M. Tapilin, Catal. Today 144 (2009) 219.
[19] J.S. McEwen, A. Garcia Cantu Ros, P. Gaspard, T. Visart de Bocarmé, N. Kruse, Catal. Today 154 (2010) 75.
[20] C.T. Herbschleb, S.C. Bobaru, J.W.M. Frenken, Catal. Today 154 (2010) 61.
[21] J.R. González-Velasco, J.A. Botas, R. Ferret, M. Pilar González-Marcos, J.L. Marc, M.A. Gutiérrez-Ortiz, Catal. Today 59 (2000) 395.
[22] L. Hannevold, O. Nilsen, A. Kjekshus, H. Fjellvåg, Appl. Catal. A: Gen. 284 (2005) 163.
[23] M. Ahmad, T.T. Tsong, J. Chem. Phys. 83 (1985) 388.
[24] A.R. McCabe, G.D.W. Smith, Platinum Met. Rev. 27 (1983) 19.
[25] T.T. Tsong, D.M. Ren, M. Ahmad, Phys. Rev. B 38 (1988) 7428.
[26] P.A.J. Bagot, A. Cerezo, G.D.W. Smith, Surf. Int. Anal. 39 (2007) 172.
[27] P.A.J. Bagot, A. Cerezo, G.D.W. Smith, Surf. Sci. 601 (2007) 2245.
[28] P.A.J. Bagot, A. Cerezo, G.D.W. Smith, Surf. Sci. 602 (2008) 1381.
[29] P.A.J. Bagot, T. Visart de Bocarmé, A. Cerezo, G.D.W. Smith, Surf. Sci. 600 (2006) 3028.
[30] J. Pérez-Ramírez, E.V. Kondratenko, G. Novell-Leruth, J.M. Ricart, J. Catal. 261 (2009) 217.
[31] D.N. Seidman, K. Stiller, MRS Bull. 34 (2009) 717.
[32] G.K. Chuah, D.L. Cocke, N. Kruse, G. Abend, J.H. Block, J. Catal. 108 (1987) 268.
[33] E.A. Marquis, T.J. Prosa, B.P. Geiser, D.J. Larson, J. Microsc. 241 (2010) 225.

[34] O.C. Hellman, J.A. Vandenbroucke, J. Rüsing, D. Isheim, D.N. Seidman, Micros. Microanal. 6 (2000) 437.
[35] W.M. Latimer, Oxidation Potentials, Prentice-Hall, 1952.
[36] D. Brennan, D.O. Hayward, B.M.W. Trapnell, Proc. R. Soc. Ser. A256 (1960) 81.
[37] K.T. Jacob, T. Uda, T.H. Okabe, Y. Waseda, High Temp. Mater. Proc. 19 (2000) 11.
[38] W.F. Gale, T.C. Totemeier, Smithells Metals Reference Book, 8th Edition, Elsevier, Oxford, 2004.
[39] L.A. Carol, G.S. Mann, Oxide Met. 34 (1990) 1.
[40] D.A. Porter, K.E. Easterling, M.Y. Sherif, Phase Transformations in Metals and Alloys, 3rd Edition, CRC Press, 2009.
[41] Y.L. He, J.K. Zuo, G.C. Wang, Surf. Sci. 255 (1991) 269.
[42] H.T. Wu, T.T. Tsong, Surf. Sci. 318 (1994) 358.
[43] W.M.H. Sachtler, R.A. van Santen, Appl. Surf. Sci. 3 (1979) 121.
[44] R.A. Van Santen, W.M.H. Sachtler, J. Catal. 33 (1974) 202.
[45] P. Wynblatt, R.C. Ku, Surf. Sci. 65 (1977) 511.
[46] F.R. de Boer, R. Boom, W.C.M. Mattens, A.R. Miedema, A.K. Niessen, Cohesion in Metals, Elsevier, Amsterdam, 1988.
[47] J. Greeley, M. Mavrikakis, Nature Mater. 3 (2004) 810.
[48] F. Tao, M.E. Grass, Y. Zhang, D.R. Butcher, J.R. Renzas, Z. Liu, J.Y. Chung, B.S. Mun, M. Salmeron, G.A. Somorjai, Science 322 (2008) 932.